STATE OF THE CLIMATE IN 2008

T. C. Peterson and M. O. Baringer, Eds.

Associate Eds.: H. J. Diamond, R. L. Fogt, J. M. Levy, J. Richter-Menge, P. W. Thorne, L. A. Vincent, and A. B. Watkins

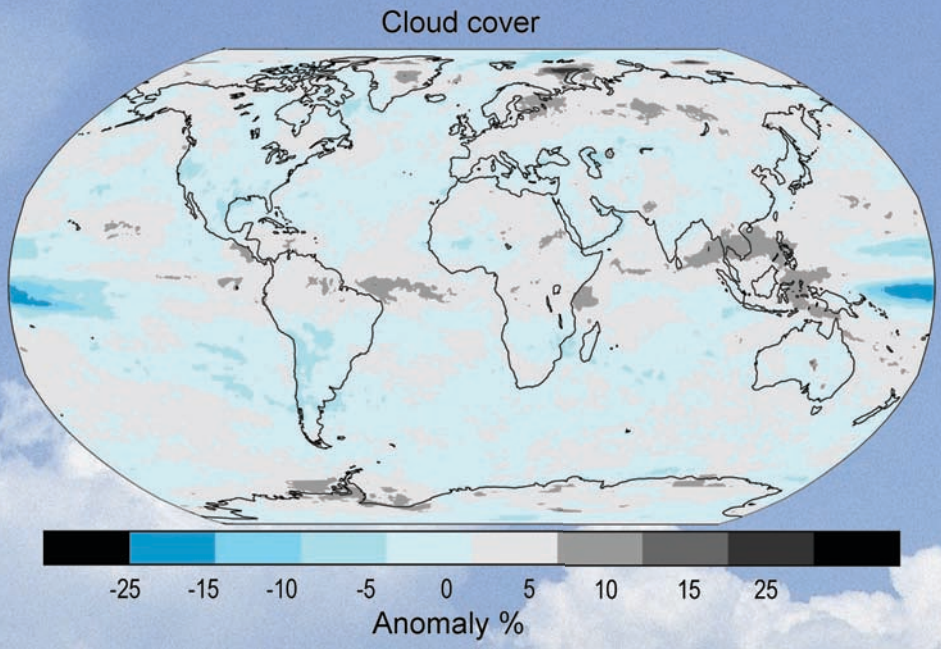

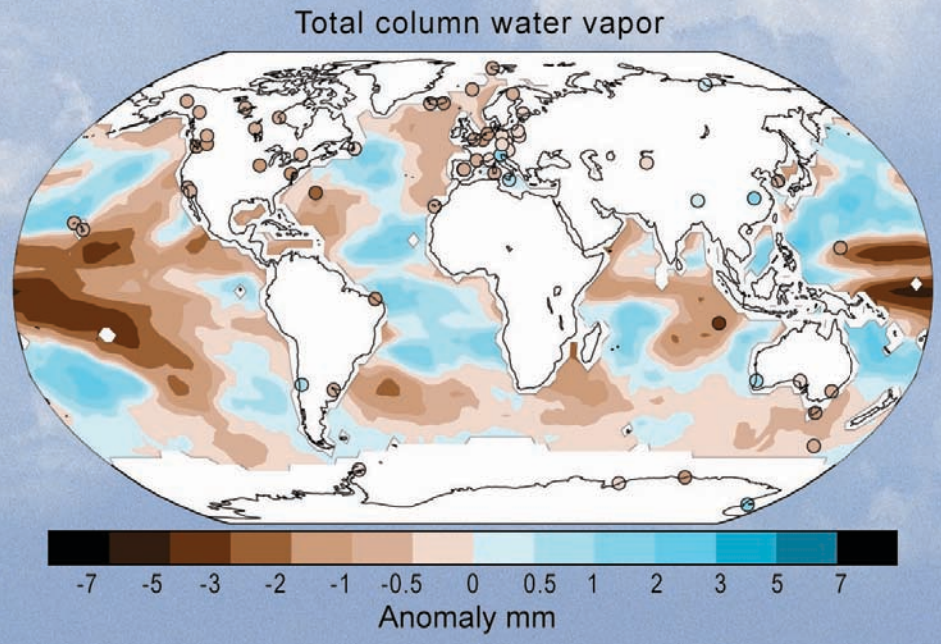

Special Supplement to the *Bulletin of the American Meteorological Society*
Vol. 90, No. 8, August 2009

HOW TO CITE THIS DOCUMENT

Citing the complete report:

Peterson, T. C., and M. O. Baringer, Eds., 2009: State of the Climate in 2008. *Bull. Amer. Meteor. Soc.*, **90,** S1–S196.

Citing a chapter (example):

Levy, J. M., Ed., 2009: Global oceans [in "State of the Climate in 2008"]. *Bull. Amer. Meteor. Soc.*, **90** (8), S1–S196.

Citing a section (example):

L'Heureux, M., G. Bell, and M. Halpert, 2009: ENSO and the tropical Pacific [in "State of the Climate in 2008"]. *Bull. Amer. Meteor. Soc.*, **90** (8)**,** S1–S196.

STATE of the CLIMATE in 2008

the radiative forcing of aerosols (Forster et al. 2007) as well as any anthropogenically influenced trend. Figure 2.32c shows the anthropogenic aerosol optical depth determined from MODIS using the retrieval algorithm of Bellouin et al. (2008). The anthropogenic aerosol optical depth consists primarily of industrial pollution (mainly sulfate, nitrate, organic carbon, and black carbon) and biomass-burning smoke (mainly volatile organic carbon, black carbon, and inorganic compounds). It averages around 0.03 over the ocean but exceeds 0.1 over many land areas.

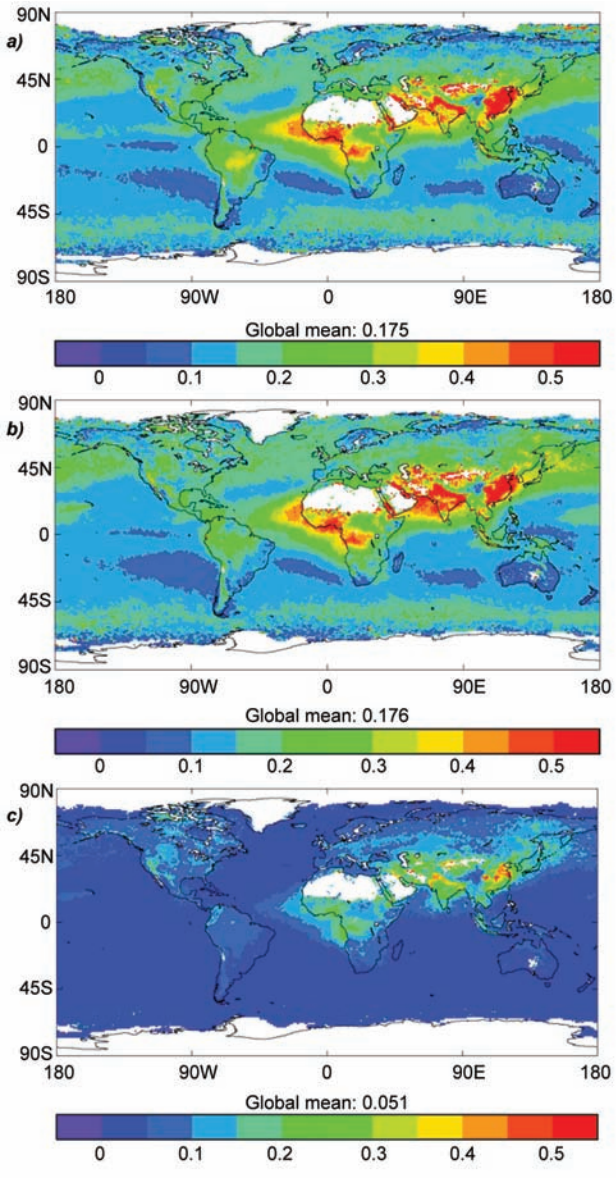

Fig. 2.32. Annual mean total aerosol optical depth derived from the MODIS *Aqua* sensor for (a) 2007, (b) 2008. (c) The anthropogenic aerosol optical depth derived from MODIS aerosol optical depths and fine-mode fractions for 2008, following Bellouin et al. (2008). Missing data areas are white.

Decreases (increases) in sulfur dioxide emissions over Europe and eastern Asia continue to be linked to increases (decreases) in surface solar radiation leading to brightening (dimming) (e.g., Wild et al. 2005). These dimming/brightening features are explicitly modeled in climate scenarios by including the effects of aerosol on radiation as shown in Fig. 2.33. Over Europe the brightening since the mid-1980s evident in the observations and in the modeling shown in Fig. 2.33 also appears well correlated with changes in atmospheric visibility (e.g., Vautard et al. 2009). The analysis of visibility trends attributes some, but not all, of the recent warming trend in the region to this phenomenon.

3) Stratospheric ozone—M. Weber

The Antarctic ozone hole area with total column ozone below 220 DU reached a maximum of 26 million km^2 by the end of September 2008; among the largest on record (www.temis.nl/protocols/o3hole/data/fd-o3area220.pdf). October total ozone above Antarctica and the tip of South America was up to 30 DU below the long-term mean. The annual anomaly was negative for most parts of the globe except for a narrow band in the tropics and a small region near the North Pole with positive anomalies of up to 10 DU (Plate 2.1, panel 9). Large negative annual anomalies were observed above Russia due to a shift of the Arctic polar vortex into this region during spring as well as lower ozone during fall. The positive tropical anomaly is related to the QBO (Baldwin et al. 2001), which was mainly in the west phase near 50 hPa. The QBO signal as well as the 11-yr solar cycle signature in the tropics is clearly evident in the total ozone anomaly time series (Fig. 2.34).

The long-term evolution of total ozone (Fig. 2.34) is dominated by lower stratospheric ozone (~30–100 hPa or 15–25 km) and can be divided into two phases. A steady decline at mid- to high latitudes from satellite record inception lasted until about the mid-1990s, followed by a sharp increase, then leveling off in recent years in the Northern Hemisphere and a leveling off with some enhanced interannual variability in the Southern Hemisphere (Fig. 2.35). Important factors are the 11-yr solar cycle, major volcanic eruptions, the QBO, and chemical ozone loss (Staehelin et al. 2001). The total ozone changes since the mid-1990s can be attributed in part to changes in the halogen load [section 2f1(iv); Dhomse et al. 2006; Froidevaux et al. 2006; Newman et al. 2006, 2007; Stolarski and Frith 2006; Yang et al. 2005]. However, changes in stratospheric circulation pattern and atmospheric dynamics, for example, Brewer–Dobson

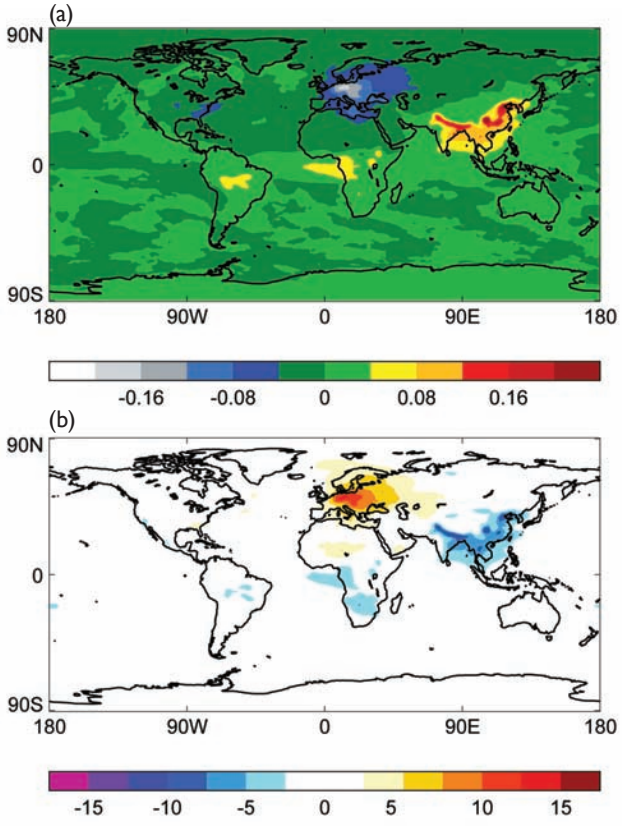

Fig. 2.33. (a) The change in aerosol optical depth simulated by the Met Office HadGEM1 over the period 1980 to 2000. Blue and gray represent a decrease in aerosol optical depths over Europe and the eastern United States due to more stringent emission controls, while red and yellow represent emissions from increasingly industrialized regions. (b) The modeled change in sunlight received at the surface (W m^{-2}) for the same period—"brightening" is shown in yellow/orange, while "dimming" is shown in the blue colors.

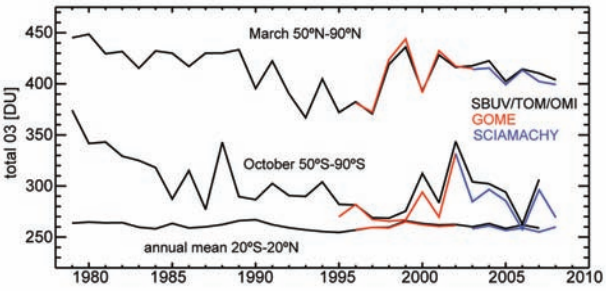

Fig. 2.34. Time series of SBUV/TOMS/OMI (black), GOME (red), and SCIAMACHY (blue) total ozone in the bands 50°–90°N in Mar, 20°S–20°N (annual mean), and 50°–90°S in Oct. Anomalies were calculated from area-weighted monthly mean zonal mean data in 5° latitude steps by removing the seasonal mean from the period 1979–89.

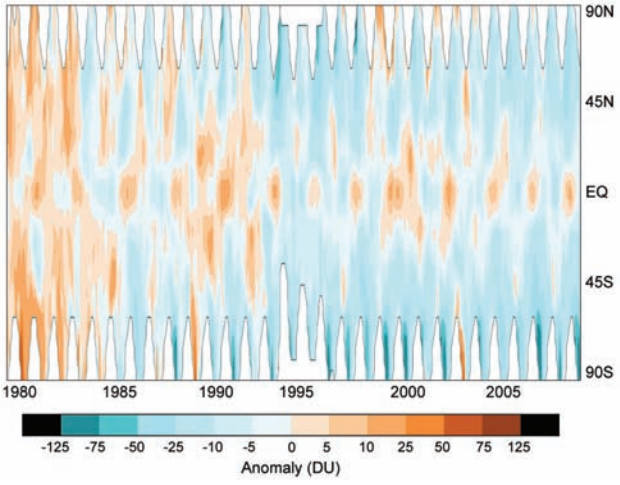

Fig. 2.35. Time variation (1979–2008) of zonally averaged total ozone anomalies. Anomalies are based on the merged SBUV/TOMS/OMI up to Jun 1995 (Frith et al. 2004), GOME from Jul 1995 to May 2003, and SCIAMACHY data from Jun 2003 to Dec 2008 (Weber et al. 2007).

circulation (Weber et al. 2003; Dhomse et al. 2006), teleconnection patterns such as the North Atlantic Oscillation (Appenzeller et al. 2000; Orsolini et al. 2004), and atmospheric advection (Wohltmann et al. 2007), all contribute to winter ozone transport from the tropical production region into middle and high latitudes and explain the large observed interannual variability in extratropical ozone (Fig. 2.35). A record-high chemical ozone loss in Arctic winter 2004/05 (Rex et al. 2006; Newman and Rex 2007) and record-size ozone hole above Antarctica in 2006 indicate that stratospheric halogen load still remains high. The rate of recovery in coming decades will strongly depend on the influence of climate change on stratospheric circulation and temperatures in addition to the expected decrease in ozone-depleting substances (Waugh et al. 2009).

The upper stratosphere is a more favorable region to investigate ozone recovery because long-term changes are larger than observed in column ozone and atmospheric dynamics are less influential (Newchurch et al. 2003). By the end of the 1990s ozone near 40-km altitude had decreased by ~8% $decade^{-1}$ at middle latitudes and then leveled off after that or slightly increased, in agreement with changes in the halogen load (Steinbrecht et al. 2009; Jones et al. 2009). In this region an eventual "super recovery" (Newman and Rex 2007) to ozone levels greater than 1960 levels can be expected if stratospheric temperatures continue to cool (Eyring et al. 2006). Surprisingly, there are indications that upper stratospheric temperatures

near 40-km altitude have not changed significantly over the past 20 yr (Steinbrecht et al. 2009), though temperature trends in this altitude region are not consistent among different datasets (section 2b3).

g. Land surface properties

1) Alpine glaciers and ice sheets—M. S. Pelto

The WGMS (WGMS 2007, 2008) provides annual global indices based on alpine glacier mass balance and terminus position, as these reflect annual volume change (Oerlemans 1994). However, a 9-month time lag prevents immediate assessment of the global state of alpine glaciers in 2008.

Worldwide retreat of mountain glaciers is one of the clearest signals of climate change (Haeberli and Hoelzel 1995). It reflects strongly negative mass balances over the last 30 yr (WGMS 2007). Mass balance is the most appropriate climate parameter for glaciers because it is an annual integral of local weather conditions (Pelto and Hedlund 2001). The change in glacier length is a smoothed and delayed response to the mass balance changes (Haeberli and Hoelzle 1995). The recent rapid retreat and prolonged negative balances have led to some glaciers disappearing (Pelto 2006).

Glacier mass balance is the difference between accumulation and ablation. Variations in temperature and/or snowfall alter the mass balance. A glacier with a sustained negative (positive) balance will retreat (advance) to reestablish equilibrium by decreasing (increasing) the area at lower elevations where ablation is highest. If a glacier lacks a consistent accumulation zone, it is in disequilibrium with climate and will disappear (Pelto 2006; Paul et al. 2007).

In 2007 the mean mass balance of all the WGMS reporting glaciers was −528-mm water equivalent; it was −673 mm for 30 reference glaciers with 30 yr of record, the 17th consecutive year of negative mass balance (Fig. 2.36a). A loss of 0.9 m of water equivalent is the same as the loss of 1.0 m of glacier thickness, since ice is less dense than water. The trend demonstrates why alpine glaciers are currently retreating. The cumulative loss of the last 30 yr (Fig. 2.36b) is the equivalent of cutting a 12–14-m-thick slice off of the average glacier. The trend is remarkably consistent from region to region (WGMS 2007), and the results from the 30 reference glaciers are not appreciably different from those for all monitored glaciers (Fig. 2.36b).

The WGMS glacier terminus position data overemphasize the European Alps, but the overall global and regional records are very similar, except for New Zealand. The proportion of advances in Europe, Asia, and North America reached a minimum in 2005 when of 442 glaciers examined, 26 advanced, 18 were stationary, and 398 (90%) retreated. Overall there has been a substantial volume loss of 11% of New Zealand glaciers from 1975 to 2005 (Salinger NWIA).

In 2008 New Zealand snowlines were 130 m above the elevation for equilibrium leading to negative mass balances and a new record minimum total ice volume for the southern Alps since records began in 1976. In Switzerland negative balances ranged from −0.6 to −1.6 m, and of the 80 glacier termini reporting to date 73 were retreating, 2 advancing, and 5 stationary (Bauder, VAW/ETH). In Norway, of 32 glaciers observed in 2008, 24 retreated, 3 advanced, and 5 were stationary (H. Elvehoi, NVE). The Pacific Northwest of North America experienced strong La Niña conditions with extra snowfall, so mass balances of North Cascade and southeast Alaska glaciers were positive in 2008.

In northern Greenland, ice melt in 2008 lasted 18 days longer than the previous maximum and the melt

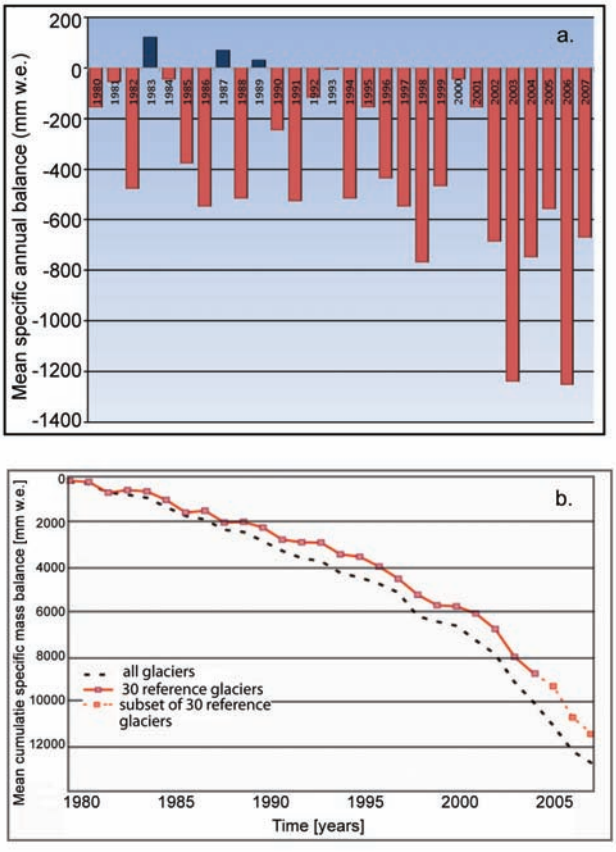

Fig. 2.36. (a) The mean annual mass balance (mm water equivalent) of 30 WGMS reference glaciers, 1980–2007. (b) The mean cumulative mass balance for the 30 reference glaciers and all monitored glaciers. The dashed line is for subset of 30 reference glaciers because not all 30 glaciers have final data for the last few years.

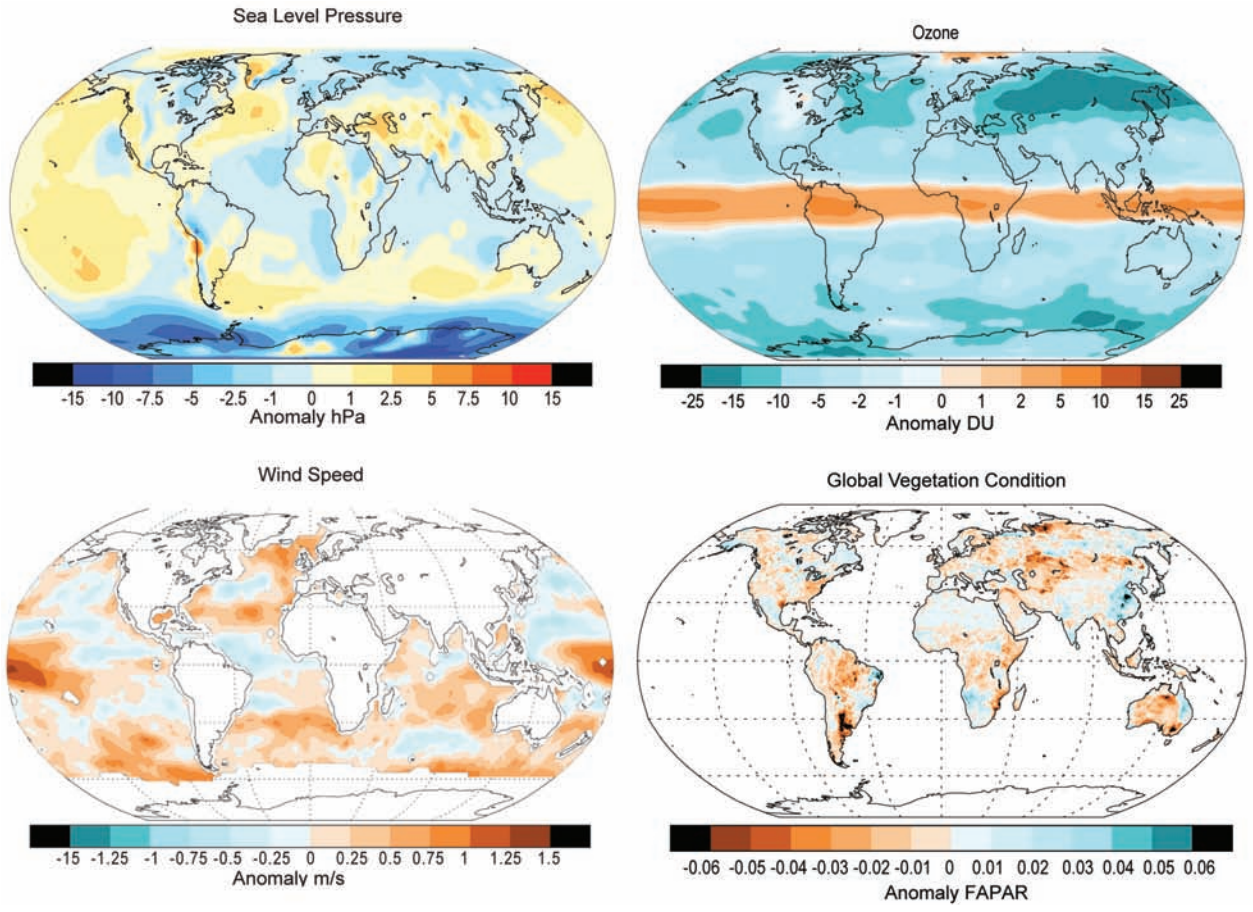

Plate 2.1. Global annual anomaly maps for those variables for which it was possible to create a meaningful anomaly estimate. Climatologies differ among variables, but spatial patterns should largely dominate over choices of climatology period. Dataset sources and climatologies are given in the form (dataset name/data source, start year–end year) for each variable. See relevant section text and figures for more details. Lower stratospheric temperature (RSS MSU 1981–90); lower tropospheric temperature (UAH MSU 1981–90); surface temperature (NCDC 1961–90); cloud cover (PATMOS-x 1982–2008); total column water vapor (SSM/I/GPS 1997–2008); precipitation (RSS/GHCN 1989–2008); mean sea level pressure (HadSLP2r 1961–90); wind speed (SSM/I 1988–2007); total column ozone (annual mean global total ozone anomaly for 2008 from SCIAMACHY. The annual mean anomalies were calculated from 1° × 1.25° gridded monthly data after removing the seasonal mean calculated from GOME (1996–2003) and SCIAMACHY (2003–07)]; vegetation condition [annual FAPAR anomalies relative to Jan 1998 to Dec 2008 from monthly FAPAR products at 0.5° × 0.5° [derived from SeaWiFS (NASA) and MERIS (ESA) data].

throughout the record. Figure 2.3 also illustrates the increase in temperatures at high latitudes of the Northern Hemisphere in recent decades. As shown in Plate 2.1, panel 3, this trend continued into 2008 when above-average temperatures were recorded across all of northern Eurasia and much of the Arctic.

2) Lower tropospheric temperatures—J. Christy, D. Seidel, C. Mears, and L. Haimberger

The 2008 global average temperature of the lower tropospheric layer (TLT, surface to ~8km) was cooler than in recent years due to the La Niña. When the surface cools, the troposphere responds with similar temperature changes, which for the global average lag the surface fluctuations by 2 to 4 months (Christy and McNider 1994). The surface was coolest in January 2008, and consequently the troposphere was coolest in May (~0.4°K below the 2007 average). Overall, 2008 was cooler than 2007 by about 0.25°K. The 51-yr time series of globally averaged TLT (Fig. 2.4) indicate this recent dip. 2008 was the 15th warmest of the mean of the datasets (individual rankings by dataset: 12th to 18th).

Datasets in Fig. 2.4 were constructed by different teams using either balloon-based radiosondes or satellite-based microwave sensors. Continuing